frontiers | Frontiers in Earth Science

TYPE Original Research
PUBLISHED 29 June 2023
DOI 10.3389/feart.2023.1112192

Check for updates

OPEN ACCESS

EDITED BY
Chris Bradley,
University of Birmingham,
United Kingdom

REVIEWED BY
Bess B. Ward,
Princeton University, United States
Xianbiao Lin,
Ocean University of China, China
Tao Huang,
Nanjing Normal University, China

*CORRESPONDENCE
Hsiao-Chun Tseng,
hctseng@email.ntou.edu.tw

†These authors have contributed equally to this work

RECEIVED 11 January 2023
ACCEPTED 20 June 2023
PUBLISHED 29 June 2023

CITATION
Tseng H-C, Yuh Han YT, Lin C-C and Gong G-C (2023), Seasonal variations of nitrous oxide in a populous urban estuary and its adjacent sea.
Front. Earth Sci. 11:1112192.
doi: 10.3389/feart.2023.1112192

Seasonal variations of nitrous oxide in a populous urban estuary and its adjacent sea

Hsiao-Chun Tseng[1,2*†], Yokie Tai Yuh Han[1†], Chia-Chia Lin[1] and Gwo-Ching Gong[1,2]

[1]Institute of Marine Environment and Ecology, National Taiwan Ocean University, Keelung, Taiwan, [2]Center of Excellence for the Oceans, National Taiwan Ocean University, Keelung, Taiwan

The first investigations of seasonal N_2O variations and water-to-air fluxes in the Tamsui River estuary and its adjacent sea were carried out in this study. In the Tamsui River estuary, the concentration of N_2O decreased with increasing salinity. The seasonal variations of N_2O concentrations in the estuary were 46.8–148.5 nM in autumn, 15.9–82.5 nM in spring, 11.0–42.0 nM in summer and 13.1–120.6 nM in winter. When salinity regressed to zero, N_2O concentration was highest in autumn, followed by winter, spring, and summer, which might be influenced by the DO and NO_3^- concentrations as well as temperature. Because of mountains occlusion, the seasonal variations in wind speed were not large in the Tamsui River estuary. Seasonal variations of N_2O fluxes in the estuary were 10.9–35.6 μmol m^{-2} d^{-1} in autumn, 2.8–15.1 μmol m^{-2} d^{-1} in spring, 2.4–9.5 μmol m^{-2} d^{-1} in summer and 2.7–26.8 μmol m^{-2} d^{-1} in winter. In the adjacent sea of Tamsui River estuary, seasonal average N_2O concentrations in the surface seawater were 10.3 ± 0.2 nM in autumn, 11.6 ± 1.2 nM in spring, 11.4 ± 0.7 nM in summer and 13.8 ± 0.9 nM in winter, with no significantly seasonal changes while wind speed varied greatly seasonally. Seasonal variations of average N_2O fluxes in Tamsui River estuary's adjacent sea were 40.3 ± 0.7 μmol m^{-2} d^{-1} in autumn, 19.7 ± 2.1 μmol m^{-2} d^{-1} in spring, 20.9 ± 1.3 μmol m^{-2} d^{-1} in summer and 49.0 ± 3.3 μmol m^{-2} d^{-1} in winter. As a result, seasonal variations in N_2O fluxes in the estuary were dominated by N_2O concentrations in the water, whereas in the sea, it was dominated by wind speed. Overall, the Tamsui River estuary and its adjacent sea were net sources of atmospheric N_2O with annual average fluxes 10.6 ± 6.7 and 32.5 ± 14.5 μmol m^{-2} d^{-1}, respectively.

KEYWORDS

Tamsui River estuary, greenhouse gas, water-to-air fluxes, nitrous oxide, N_2O, urban estuary

1 Introduction

Nitrous oxide (N_2O), one of the most important greenhouse gases in the world, has a global warming potential approximately 300 times that of carbon dioxide (IPCC, 2013). It has also become the most important ozone-depleting substance since the restriction of chlorofluorocarbon (CFC) enforced by the Montreal Protocol (Ravishankara et al., 2009). Observational data noted that atmospheric N_2O concentration has risen from 270 ppb in the year 1750 (pre-industrial level) to 332 ppb in 2019 (IPCC, 2021). Human activities have enhanced atmospheric N_2O concentrations by approximately 23%

compared to pre-industrial levels, and the growth rate has been higher in recent years (IPCC, 2021).

According to the Intergovernmental Panel on Climate Change (IPCC) Fifth Assessment Report (AR5), N_2O is emitted from both anthropogenic and natural sources. Natural sources of N_2O include microbial processes in land and ocean. The total flux of natural sources was about 11 TgN yr^{-1} and the ocean contributed about 30% of N_2O (3.8 TgN yr^{-1}) to the atmosphere (IPCC, 2013). In recent decades, emissions from natural sources have not changed much, but emissions resulting from anthropogenic activities have grown by 30% over the past three decades (Tian et al., 2020). Anthropogenic sources of N_2O fluxes were about 6.9 TgN yr^{-1}, which includes agriculture, rivers, estuaries, human excreta, fossil fuels and industry, biomass and biofuel burning, and atmospheric deposition on land and ocean. Rivers and estuaries are potentially substantial global sources of N_2O (Seitzinger and Kroeze, 1998). As N_2O emissions from estuaries and oceans could be significant and should not be disregarded, obtaining high-resolution data on these emissions is crucial to refine the calculation of nitrogen budget.

Urbanization around rivers and estuaries will increase the emissions of N_2O (Reading et al., 2020). In addition, land-use changes not only affect water column N_2O emissions but also have a considerable influence on benthic N_2O production, and increasing land-use intensity could accelerate N_2O emissions to the atmosphere (Chen et al., 2022). The Tamsui River is an urban river highly affected by anthropogenic activities. Here, we provide the first dataset of N_2O studies in the Tamsui River estuary and its adjacent sea area.

2 Materials and methods

2.1 Study area

The Tamsui River is located in the northern part of Taiwan and is formed by the three tributaries of the Dahan, Xindian and Keelung Rivers. It has a total length of 159 km and a catchment area of approximately 2,726 km^2. The regional climate is subtropical. The temperature in this region varies between 10°C and 35°C and annual precipitation ranges between 1500 and 2,500 mm (Wen et al., 2008). From November to April is the dry season with the average rainfall over past 25 years (1995–2020) 776 ± 269 mm, and from May to October is the wet season with the average rainfall over past 25 years (1995–2020) 1322 ± 440 mm (Central Weather Bureau: https://www.cwb.gov.tw/eng/). There were 7.13 million people, were about 30% population of Taiwan living in the Tamsui River catchment, and the regional population density can reach as high as 38,607 people per km^2 (Tseng et al., 2021). In the past 10 years, pollution sources have been controlled, and the water quality of the river basin has improved remarkably (Tseng et al., 2021). However, Tamsui River is still polluted by both raw sewage and industrial pollution. According to the Tamsui River monitoring data in 2019, it was approximately 8.3% slightly polluted, 15.9% moderately polluted and 2.6% severely polluted (TEPA, 2021). Long-term observation is needed to maintain good conditions of the Tamsui River, the Tamsui River estuary, and its adjacent sea area.

2.2 Field sampling

In the Tamsui River estuary, surface water samples were collected at seven sampling stations in a small fishing boat using a plastic bucket with rope, in the same sampling month as its adjacent sea, in November 2019 May 2020, August 2020, and January 2021. Temperature data were measured onboard using a thermometer, whereas salinity values were determined by measuring conductivity using an AUTOSAL salinometer (8400B, Guildline Instruments Ltd., Canada) in the laboratory.

In the Tamsui River estuary adjacent sea area (Figure 1), four seasonal research cruises were conducted onboard R/V Ocean Researcher 2 and R/V New Ocean Researcher 2: OR2-2390 (November 2019), NOR2-0004 (May 2020), NOR2-0009 (August 2020), and NOR2-0027 (January 2021). Surface water samples were collected at 16 sampling stations in autumn (November 2019) and 20 sampling stations in spring (May 2020) and summer (August 2020). In winter (January 2021), because of adverse weather conditions, surface water samples were only taken at 10 sampling stations. Water samples were collected using a carousel water sampler (SBE32, Seabird Scientific, United States) fitted with 20 L Teflon-coated Go-Flo bottles (General Oceanic, United States) mounted on a conductivity–temperature–depth instrument (CTD; SBE 9/11 plus, Seabird Scientific, United States) assembly. Temperature and salinity data were obtained from CTD profiles.

Water samples for nutrients analysis were filtered and placed in 100 mL polypropylene bottles and immediately frozen with liquid nitrogen. Water samples that were used to measure N_2O concentrations were collected in 120 mL dark borosilicate serum bottles. The bottles were rinsed thrice using sampled water. After two-fold of the bottle was allowed to overflow, 0.2 mL saturated $HgCl_2$ was then added. The sample bottles were immediately sealed with a butyl rubber stopper and an aluminum cap. The samples were stored in a dark box at 4°C. All water samples were transferred to the laboratory and analyzed within 3 months of collection.

2.3 Chemical analysis

Dissolved oxygen (DO) was measured using spectrophotometry (Pai et al., 1993) with a precision of approximately ±0.32% at the 190 μmol L^{-1} level. Nitrate (NO_3^-) and nitrite (NO_2^-) concentrations were measured by the pink azo dye method (Strickland and Parsons, 1972) using a flow injection analyzer and an online Cd coil. NO_2^- concentration was also determined by the pink azo dye method (Strickland and Parsons, 1972; Pai et al., 1990b) using a flow injection analyzer. The precisions of NO_3^- and NO_2^- were ±0.3 and ±0.02 μmol L^{-1}, respectively. Phosphate (PO_4^{3-}) was determined under the molybdenum blue method (Murphy and Riley, 1962; Pai et al., 1990a) using a flow injection analyzer. The precision of the measurements was approximately ±0.01 μmol L^{-1}. NH_4^+ was measured using an improved indophenol blue method (Pai et al., 2001) with a precision of approximately 1% at the 5 μmol L^{-1} level.

N_2O measurements were performed using the headspace technique (Weiss, 1981) and gas chromatography (GC; Agilent 7890) with an electron capture detector (ECD). The GC-ECD had a 3.6 m long stainless-steel column with a diameter of

10.3389/feart.2023.1112192

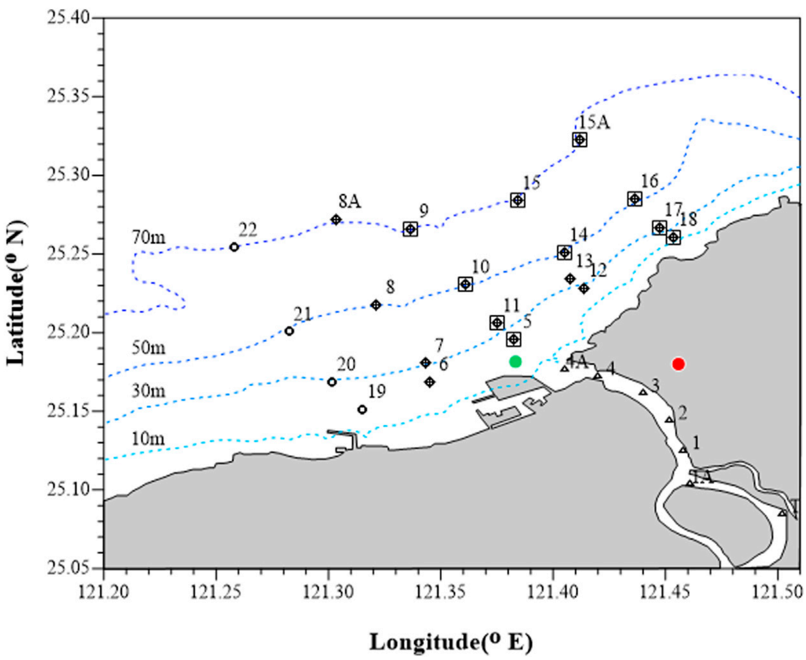

FIGURE 1
Study area and station locations. +: OR2-2390 (November 2019, Autumn); ○: NOR2-0004 (May 2020, Spring) and NOR2-0009 (August 2020, Summer); □: NOR2-0027 (January 2021, Winter). Δ: Stations in Tamsui River estuary. Green dot: Wind speed station of Institute of Harbor and Marine Technology (IHMT). Red dot: Tamsui Weather Station of Central Weather Bureau (CWB).

3.2 mm, which was filled with 80/100 mesh Porapak Q. The temperature of ECD was set as 300°C and was calibrated with pure N_2 (Yeong Her, Taiwan) and three commercial gas mixtures with N_2O mixing ratios of 1.00 ppmv (MESA Specialty Gas, United States), 4.78 ppmv (Yeong Her, Taiwan) and 9.90 ppmv (Yeong Her, Taiwan). The reproducibility of measurements was ±3% for N_2O.

2.4 N_2O saturation ratio and fluxes

The saturation (R, %) and sea-to-air flux (F, μmol·m^{-2}·d^{-1}) of N_2O were calculated using the following formula:

$$R = \left(C_{obs}/C_{eq}\right) \times 100$$

$$F\ (\mu mol{\cdot}m^{-2}{\cdot}d^{-1}) = k\ (C_{obs} - C_{eq})$$

$$k = 0.251 \times u^2 \times (Sc/660)^{-1/2}$$

where C_{obs} is the observed concentration of N_2O dissolved in water and C_{eq} is the expected equilibrium water N_2O concentration. The expected equilibrium water concentration was calculated using the solubility equation of Weiss and Price (1980) together with the *in situ* temperature, salinity, and molar fraction of N_2O in the air. Atmospheric N_2O concentrations were obtained using the NOAA/ESRL *in situ* program (http://www.esrl.noaa.gov/gmd). The monthly average atmospheric N_2O concentrations at Mauna (Hawaii, United States station) were 331.6, 334.0, 334.1, and 334.3 ppb in November 2019 May 2020, August 2020, and January 2021, respectively. The gas exchange coefficient k was calculated using the equation established by Wanninkhof (2014), where Sc is the Schmidt number of N_2O and u represents the wind speed.

Monthly average wind speed data for calculating fluxes of N_2O in the Tamsui River estuary were provided by the Central Weather Bureau: https://e-service.cwb.gov.tw/HistoryDataQuery/index.jsp and for the Tamsui River's adjacent sea were obtained from the Institute of Harbor and Marine Technology: https://isohe.ihmt.gov.tw/docklands/reportR.aspx.

3 Results

Seasonal hydrographic and nutrient data, as well as N_2O concentrations, were measured in the Tamsui River estuary and its adjacent sea. Detailed information on seasonal sampling in the Tamsui River estuary and its adjacent sea as well as the range of hydrographic data, nutrients, and N_2O concentrations in the surface water are listed in Table 1.

3.1 Aquatic environmental conditions and N_2O concentrations in autumn

In autumn, the surface temperature ranged between 23.0°C and 24.0°C in the Tamsui River estuary, and it was similar with the average surface temperature, 23.8°C ± 0.2°C (Table 1), in the adjacent sea (Figure 2A). The surface water salinity gradually increased from the estuary to the coast (Figure 2B). The range of surface salinity were between 0.70 and 19.08 in the Tamsui River

10.3389/feart.2023.1112192

TABLE 1 Seasonal hydrographic data, nutrients and N_2O concentrations in the surface water of both Tamsui River estuary and its adjacent sea.

Season	Tamsui River estuary and its adjacent	Temperature	Salinity	N_2O	N_2O saturation	DO	DO saturation	NH_4^+	NO_2^-	NO_3^-	PO_4^{3-}
		(˚C)		(nM)	(%)	(μM)	(%)	(μM)	(μM)	(μM)	(μM)
Autumn 2019 November	Estuary	23.0–24.0	0.70–19.08	46.8–148.5	582–1808	208.4–226.2	80–96	100.7–180.6	7.63–9.62	28.2–45.2	3.16–7.42
	Adjacent sea	23.8 ± 0.2	33.63 ± 0.10	10.3 ± 0.2	148 ± 3	221.4 ± 3.4	102 ± 2	0.9 ± 0.9	0.52 ± 0.36	3.8 ± 0.6	0.37 ± 0.08
Spring 2020 May	Estuary	26.0–28.7	5.69–32.14	15.9–82.5	244–1101	106.6–206.3	44–98	22.3–104.4	7.00–35.07	ND	1.20–7.11
	Adjacent sea	26.8 ± 0.2	33.83 ± 0.55	11.6 ± 1.2	183 ± 18	206.4 ± 5.8	100 ± 3	3.8 ± 2.7	0.36 ± 0.29	1.1 ± 0.9	0.35 ± 0.20
Summer 2020 August	Estuary	30.0–31.0	14.49–33.87	11.0–42.0	194–679	141.1–197.0	65–101	2.5–106.6	2.03–40.60	0.0–0.2	0.35–5.58
	Adjacent sea	29.9 ± 0.7	33.89 ± 0.16	11.4 ± 0.7	197 ± 12	192.7 ± 5.7	98 ± 3	2.0 ± 1.2	0.33 ± 0.12	1.1 ± 0.6	0.29 ± 0.11
Winter 2021 January	Estuary	15.5–18.0	1.35–33.08	13.1–120.6	149–1158	195.2–249.4	64–102	5.2–69.7	6.07–49.19	2.8–17.6	1.04–4.74
	Adjacent sea	18.8 ± 0.4	33.75 ± 0.53	13.8 ± 0.9	171 ± 11	243.7 ± 8.5	103 ± 4	1.2 ± 1.5	1.07 ± 0.44	6.7 ± 0.5	0.61 ± 0.12

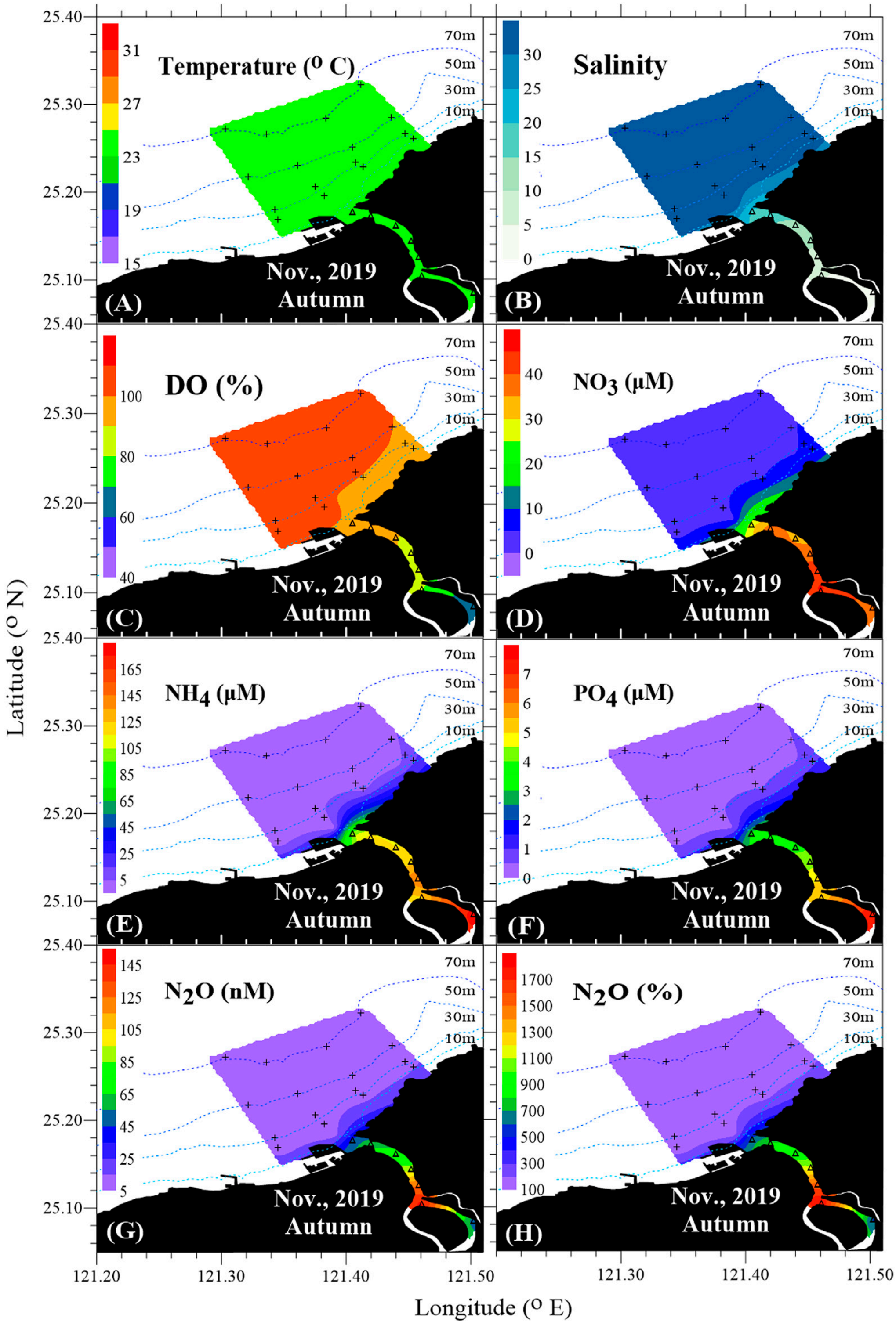

FIGURE 2
Horizontal distributions of the surface water in the Tamsui River estuary and its adjacent sea during autumn, including **(A)** Temperature, **(B)** Salinity, **(C)** DO%, **(D)** NO_3^-, **(E)** NH_4^+, **(F)** PO_4^{3-}, **(G)** N_2O, **(H)** N_2O%.

estuary and it increased to the average of 33.63 ± 0.10 (Table 1) in the adjacent sea. The surface DO saturation was between 80% and 96% (Table 1) in the Tamsui River estuary and it increased from estuary to the coast (Figure 2C). The average DO saturation was 102% ± 2% (Table 1) in the adjacent sea. In the estuary, NO_3^-, NH_4^+, and PO_4^{3-} concentrations ranged from 28.2 to 45.2 μM, 100.7–180.6 μM, and 3.16–7.42 μM (Table 1), respectively. The highest NO_3^-, NH_4^+, and PO_4^{3-} concentrations were observed in

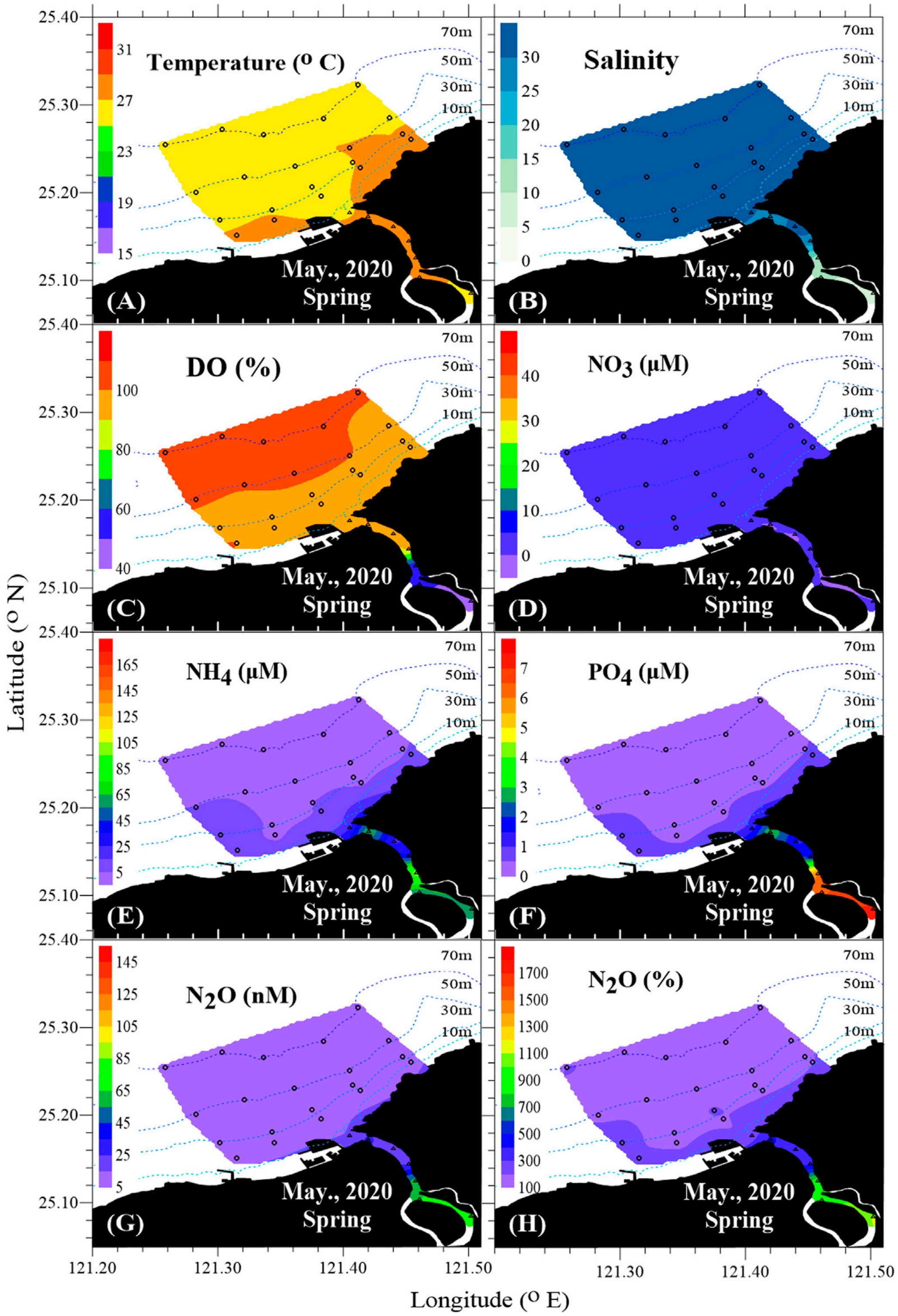

FIGURE 3
Horizontal distributions of the surface water in the Tamsui River estuary and its adjacent sea during spring, including **(A)** Temperature, **(B)** Salinity, **(C)** DO%, **(D)** NO_3^-, **(E)** NH_4^+, **(F)** PO_4^{3-}, **(G)** N_2O, **(H)** N_2O%.

the river tributaries and then gradually decreased in the estuary and adjacent sea (Figures 2D–F). The average concentrations of NO_3^-, NH_4^+, and PO_4^{3-} in the surface water of the Tamsui River adjacent sea were 3.8 ± 0.6 μM, 0.9 ± 0.9 μM, and 0.37 ± 0.08 μM (Table 1), respectively. In the Tamsui River estuary, dissolved N_2O concentrations, and saturations ranged from 46.8 to

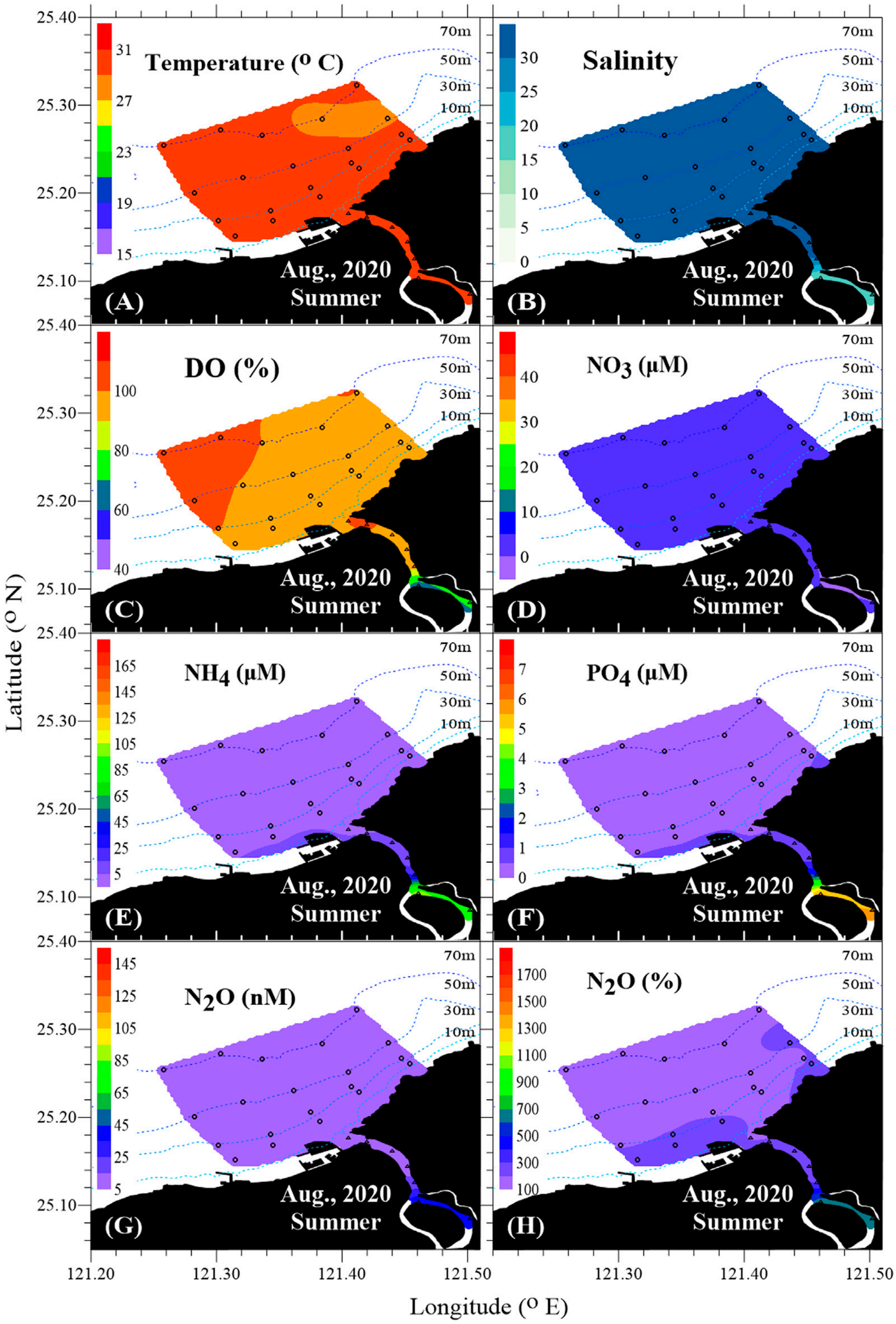

FIGURE 4
Horizontal distributions of the surface water in the Tamsui River estuary and its adjacent sea during summer, including **(A)** Temperature, **(B)** Salinity, **(C)** DO%, **(D)** NO_3^-, **(E)** NH_4^+, **(F)** PO_4^{3-}, **(G)** N_2O, **(H)** N_2O%.

148.5 nM and 582%–1808% (Table 1), respectively. The highest N_2O concentration was in the confluence of river tributaries, where the highest NO_3^- concentration was observed, which then decreased from the estuary to the coast (Figure 2G). In the Tamsui River adjacent sea, dissolved N_2O concentration in the surface water was distributed evenly and the average

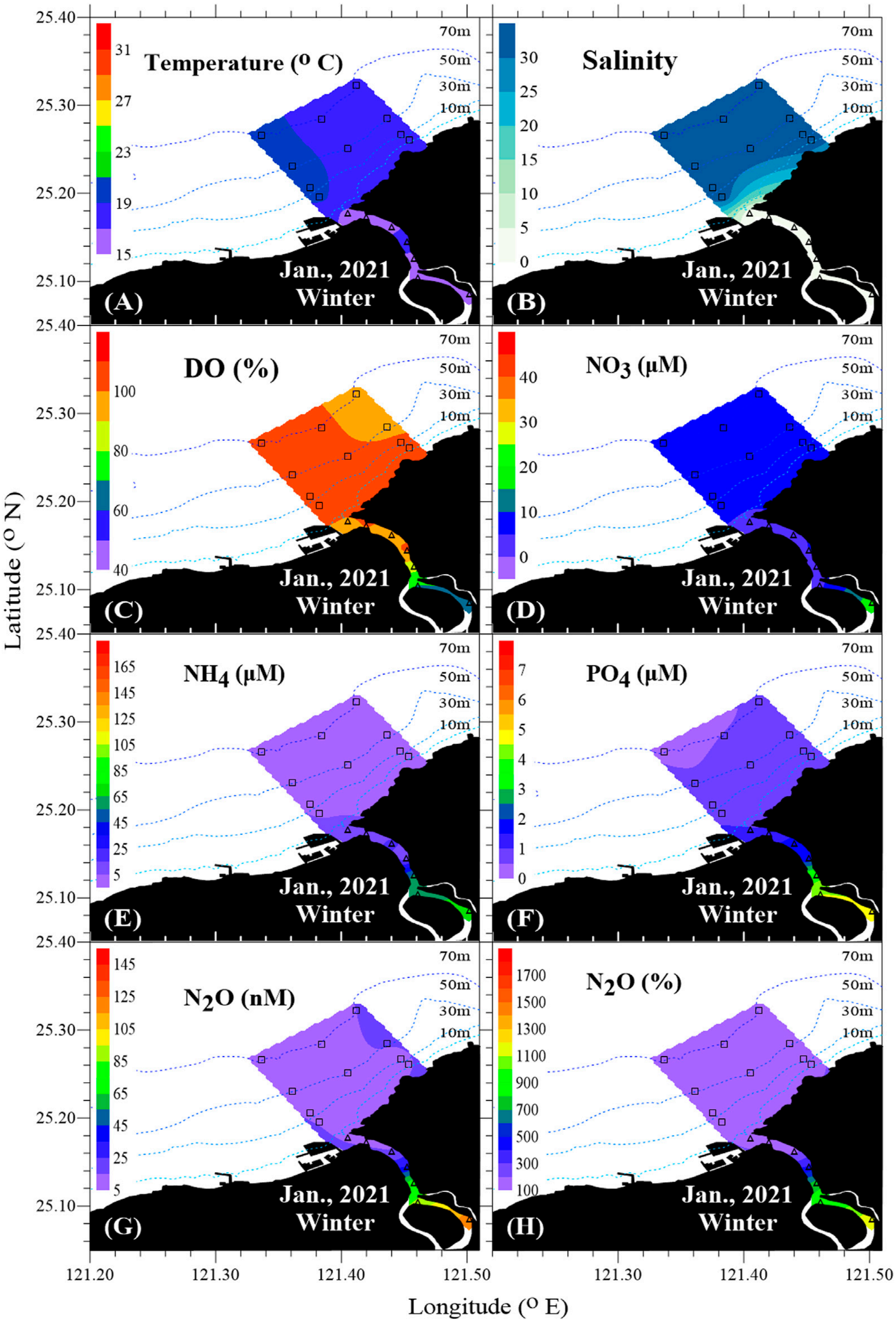

FIGURE 5
Horizontal distributions of the surface water in the Tamsui River estuary and its adjacent sea during winter, including **(A)** Temperature, **(B)** Salinity, **(C)** DO%, **(D)** NO_3^-, **(E)** NH_4^+, **(F)** PO_4^{3-}, **(G)** N_2O, **(H)** N_2O%.

concentration was 10.3 ± 0.2 nM (Table 1). N_2O was supersaturated in the Tamsui River estuary and then decreased from the estuary to the coast owing to physical mixing (Figure 2H). In the Tamsui River adjacent sea, N_2O was slightly oversaturated, with average saturation 148% (Table 1).

TABLE 2 Seasonal N_2O concentrations, wind speed, N_2O fluxes in surface water of both Tamsui River estuary and its adjacent sea.

Season	Atmospheric N_2O concentration (ppb)	Estuary			Sea		
		N_2O concentration (nM)	Wind speed (m s^{-1})	N_2O flux (μmol $m^{-2}d^{-1}$)	N_2O concentration (nM)	Wind speed (m s^{-1})	N_2O flux (μmol $m^{-2}d^{-1}$)
Autumn (Nov. 2019)	331.6	46.8–148.5	1.9 ± 0.7	10.9–35.6	10.3 ± 0.2	7.9 ± 0.8	40.3 ± 0.7
Spring (May 2020)	334.0	15.9–82.5	1.6 ± 0.6	2.8–15.1	11.6 ± 1.2	5.0 ± 0.6	19.7 ± 2.1
Summer (Aug. 2020)	334.1	11.0–42.0	1.7 ± 0.8	2.4–9.5	11.4 ± 0.7	5.0 ± 0.7	20.9 ± 1.3
Winter (Jan. 2021)	334.4	13.1–120.6	2.0 ± 0.7	2.8–26.8	13.8 ± 0.9	8.0 ± 0.8	49.0 ± 3.3

The monthly average atmospheric N_2O concentrations were taken from the NOAA/ESRL, *in situ* program (Mauna, Hawaii, United States).
Averaged monthly wind speeds in the estuary was obtained from the Tamsui Weather Station of Central Weather Bureau.
Averaged monthly wind speeds in the sea was obtained from the Wind Speed Station of Institute of Harbor and Marine Technology.
Fluxes were calculated by Wanninkhof (2014) equation.

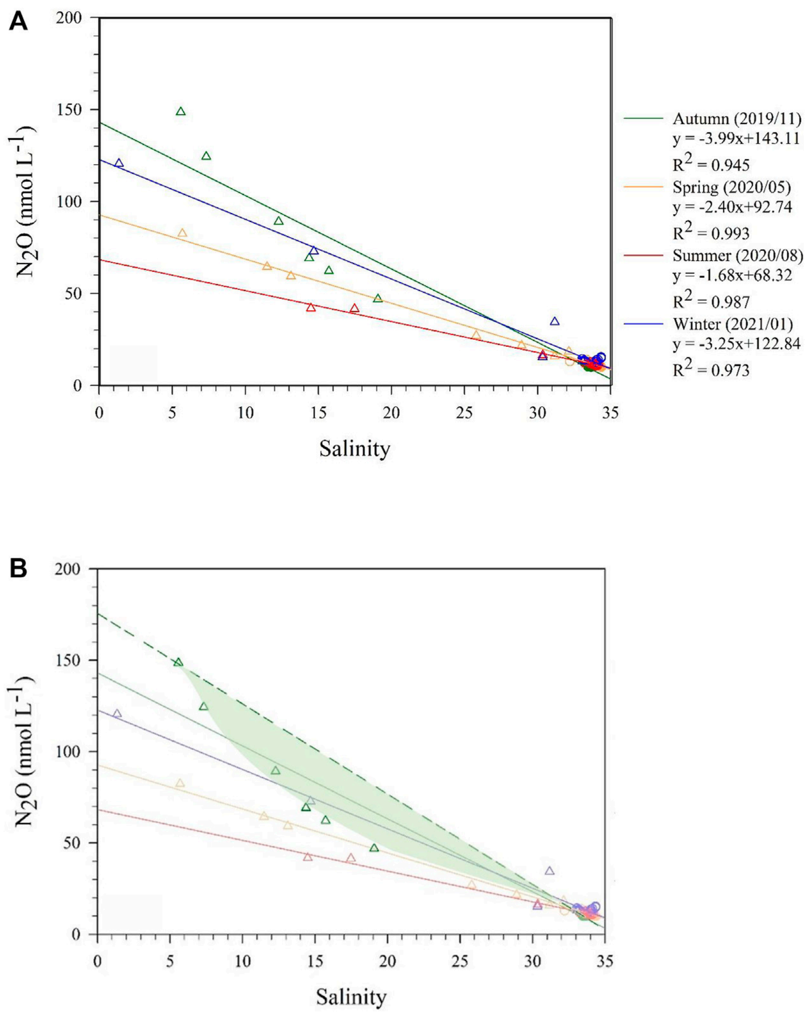

FIGURE 6
(A) Four seasonal surface N_2O concentration *versus* salinity from Tamsui River estuary to adjacent sea. **(B)** In autumn, the shaded area showed N_2O concentrations might be removed during transportation. (O: data from the adjacent sea, Δ: data from Tamsui River estuary).

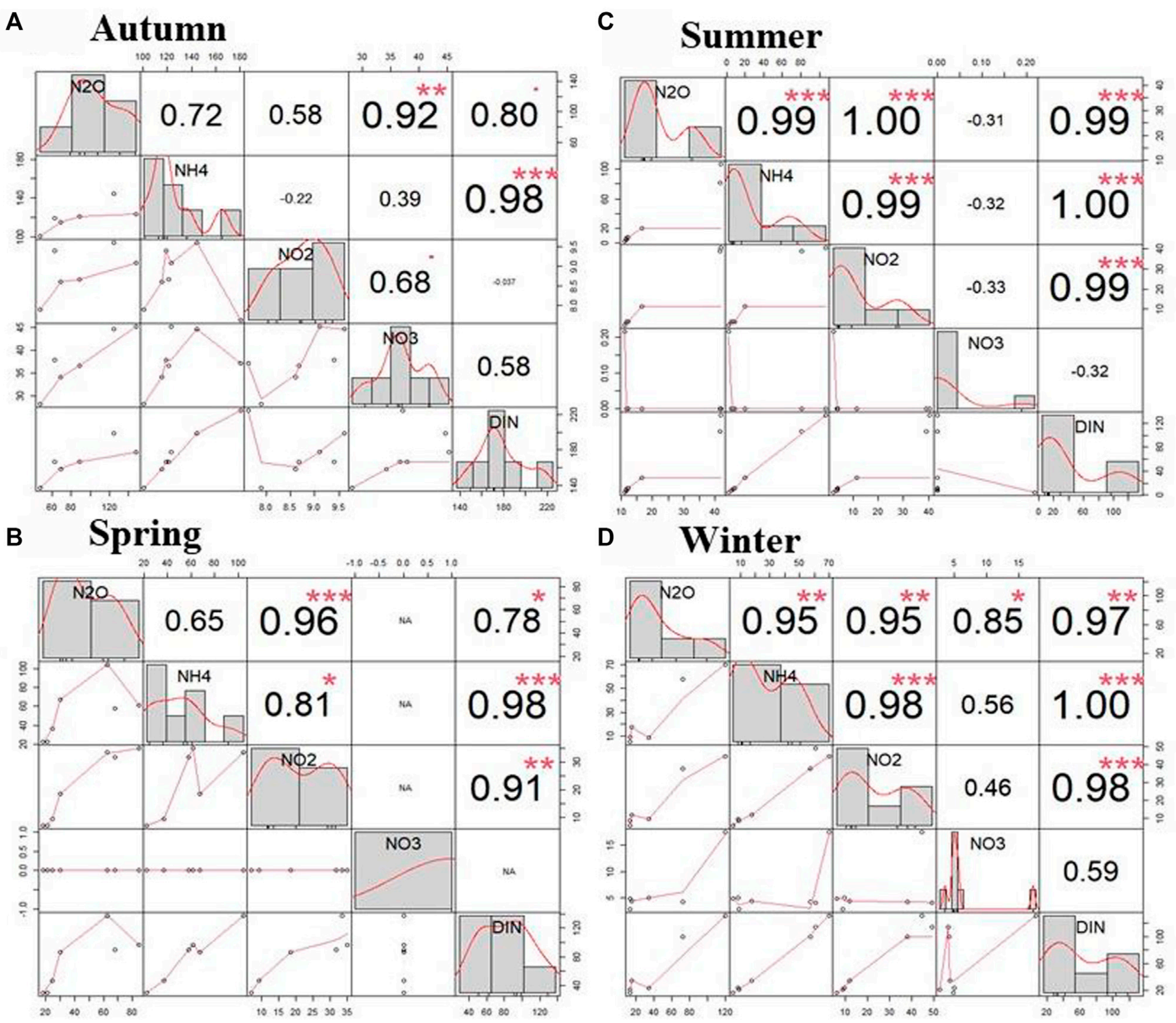

FIGURE 7
The Pearson correlations between N_2O, NH_4^+, NO_2^-, NO_3^- and DIN in **(A)** autumn **(B)** spring **(C)** summer **(D)** winter. Diagonal shows the distribution of the variable. The upper triangle of the matrix shows correlation values (r values) and *, **, *** indicate statistical significance (*p*-values) at $p< 0.05$, $p<0.01$, $p<0.001$. The lower triangle of the matrix shows the scatter distribution of variables.

3.2 Aquatic environmental conditions and N_2O concentrations in spring

In spring, the range of surface temperature were between 26.0°C and 28.7°C in the Tamsui River estuary, and it was slightly higher than its adjacent sea (Figure 3A), with average surface temperature 26.8°C ± 0.2°C (Table 1). The surface water salinity gradually increased from the estuary to the coast (Figure 3B). The range of surface salinity was between 5.69 and 32.14 in the Tamsui River estuary and it increased to an average of 33.83 ± 0.55 (Table 1) in its adjacent sea. The surface DO saturation was between 44% and 98% (Table 1) in the Tamsui River estuary and it increased from estuary to the coast (Figure 3C). The average DO saturation was 100% ± 3% (Table 1) in the adjacent sea. Concentrations of NO_3^- were considered low in both the estuary and its adjacent sea (Figure 3D) and in the estuary were below the detection limit (Table 1). In the estuary, NH_4^+ and PO_4^{3-} concentrations ranged from 22.3 to 104.4 μM and 1.20–7.11 μM (Table 1), respectively. The highest NH_4^+ and PO_4^{3-} concentrations were observed in the river tributaries and then gradually decreased in the estuary and adjacent sea (Figures 3E,F). The average concentrations of NO_3^-, NH_4^+, and PO_4^{3-} in the Tamsui River adjacent sea were 1.1 ± 0.9 μM, 3.8 ± 2.7 μM, and 0.35 ± 0.20 μM (Table 1), respectively. In the Tamsui River estuary, dissolved N_2O concentrations and saturations ranged from 15.9 to 82.5 nM and 244%–1101% (Table1), respectively. Dissolved N_2O concentration in the surface water decreased from estuary to the adjacent sea (Figure 3G) and the average dissolved N_2O concentration in the adjacent sea was 11.6 ± 1.2 nM (Table 1). N_2O was supersaturated in the Tamsui River estuary and decreased from the estuary to the coast (Figure 3H). In the Tamsui River adjacent sea, N_2O was oversaturated, with average saturation 183% ± 18% (Table 1).

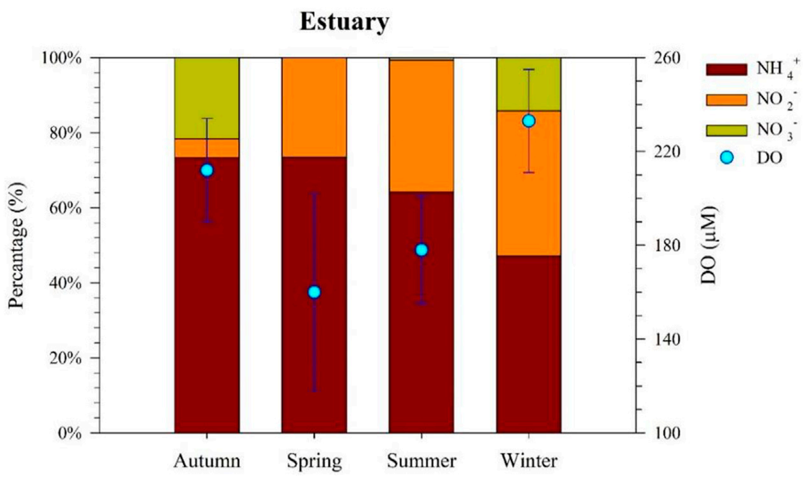

FIGURE 8
Seasonal variation of dissolved inorganic nitrogen (DIN) proportion (%) and DO (μM) in Tamsui River estuary. (*DIN = NO_2^- + NO_3^- + NH_4^+).

3.3 Aquatic environmental conditions and N_2O concentrations in summer

In summer, the range of surface temperature was between 30.0°C and 31.0°C in the Tamsui River estuary, which was similar to the average surface temperature of 29.9°C ± 0.7°C in the adjacent sea (Figure 4A). The surface water salinity gradually increased from the estuary to the coast (Figure 4B). The range of surface salinity was between 14.49 and 33.87 in the Tamsui River estuary and it increased to an average of 33.89 ± 0.16 (Table 1) in the adjacent sea. The surface DO saturation was between 65% and 101% (Table 1) in the Tamsui River estuary and it increased from estuary to the coast (Figure 4C). The average DO saturation was 98% ± 3% (Table 1) in the adjacent sea. In the estuary, NO_3^-, NH_4^+, and PO_4^{3-} concentrations ranged from 0.0 to 0.2 μM, 2.5–106.6 μM, and 0.35–5.58 μM (Table 1), respectively. The concentrations of NO_3^- were low throughout the estuary and adjacent sea (Figure 4D). The highest NH_4^+ and PO_4^{3-} concentrations were observed in the river tributaries and then gradually decreased in the estuary and adjacent sea (Figures 4E,F). The average concentrations of NO_3^-, NH_4^+, and PO_4^{3-} in the Tamsui River adjacent sea were 1.1 ± 0.6 μM, 2.0 ± 1.2 μM, and 0.29 ± 0.11 μM (Table 1), respectively. In the Tamsui River estuary, dissolved N_2O concentrations and saturations were ranged from 11.0 to 42.0 nM and 194% to 679% (Table1). N_2O decreased from estuary to the coastal area due to physical mixing (Figure 4H). In the Tamsui River adjacent sea, dissolved average surface N_2O concentration was 11.4 ± 0.7 nM and saturation was 197% ± 12% (Table 1).

3.4 Aquatic environmental conditions and nitrous oxide concentrations in winter

In winter, owing to adverse weather conditions, only 10 stations were sampled. The surface temperature ranged between 15.5°C and 18.0°C in the Tamsui River estuary was slightly lower than the average surface temperature, 18.8°C ± 0.4°C, in the adjacent sea (Figure 5A). The surface salinity ranged between 1.35 and 33.08 in the Tamsui River estuary and the average surface salinity was 33.75 ± 0.53 (Table 1) in the adjacent sea. The surface DO saturation was between 64% and 102% (Table 1) in Tamsui River estuary and it increased from the estuary to the coast (Figure 5C). The average DO saturation was 103% ± 4% (Table 1) in the adjacent sea. In the estuary, NO_3^-, NH_4^+, and PO_4^{3-} concentrations ranged from 2.8 to 17.6 μM, 5.2–69.7 μM, and 1.04–4.74 μM (Table 1), respectively. The highest NO_3^-, NH_4^+, and PO_4^{3-} concentrations were observed in the river tributaries and then gradually decreased in the estuary and adjacent sea (Figures 5D–F). The average surface concentrations of NO_3^-, NH_4^+, and PO_4^{3-} in the Tamsui River adjacent sea were 6.7 ± 0.5 μM, 1.2 ± 1.5 μM, and 0.61 ± 0.12 μM (Table 1), respectively. In the Tamsui River estuary, dissolved N_2O concentrations and saturations were ranged from 13.1 to 120.6 nM and 149% to 1158% (Table 1), respectively. The highest N_2O concentration was observed in the upper estuary (Figure 5G). In the Tamsui River adjacent sea, higher dissolved N_2O concentration occurred at northern site and the average concentration was 13.8 ± 0.9 nM (Table 1). N_2O was supersaturated in the Tamsui River estuary and decreased from the estuary to the coast (Figure 5H). In the Tamsui River adjacent sea, N_2O was oversaturated, with average saturation 171% ± 11% (Table 1).

4 Discussion

4.1 Seasonal changes of water conditions in the Tamsui River estuary and its adjacent sea

The surface water temperature in the Tasmsui River estuary was highest in summer (30.0°C–31.0°C), followed by spring (26.0°C–28.7°C) and autumn (23.0°C–24.0°C), and lowest in winter (15.5°C–18.0°C; Table 1). The surface temperature in Tamsui River estuary's adjacent sea during four seasons, in descending order, was summer (29.9°C ± 0.7°C), spring (26.8°C ± 0.2°C), autumn (23.8°C ± 0.2°C), and winter (18.8°C ± 0.4°C; Table 1). Seasonal changes in surface temperature were in both the estuary and adjacent sea. In estuaries, salinity typically represents tidal effects. As salinity in the estuary and its adjacent sea were

TABLE 3 N_2O fluxes in rivers and estuaries.

Location	Time	Salinity	N_2O saturation (%)	N_2O flux (μmol m^{-2} d^{-1})	References
Coffs creek	2016, Mar (dry)	0.1–37.5	133.1–281.0	4.0–28.0[a]	Reading et al. (2020)
	2016, Jun (wet)	0.0–35.3	85.6–677.7	−1.2–120.9[a]	
Boambee creek	2016, Mar (dry)	0.1–37.1	112.9–291.8	1.5–29.9[a]	
	2016, Jun (wet)	0.1–34.6	87.4–329.0	−1.2–26.2[a]	
Bonville creek	2016, Mar (dry)	0.1–34.7	77.7–309.7	−2.8–31.2[a]	
	2016, Jun (wet)	0.1–29.0	136.8–286.5	2.6–19.4[a]	
Pine creek	2016, Mar (dry)	0.1–34.7	78.7–201.2	−2.7–17.0[a]	
	2016, Jun (wet)	0.0–29.0	136.8–381.5	2.6–29.8[a]	
Parramatta River	2018, May	25.5–32.5	100–171	−0.6–11.0[b]	
Upper Central Sydney Harbour	2018, May	28.7–35.6	91–154	−0.8–3.5[b]	Reading (2022)
Lower Central Sydney Harbour	2018, May	32.5–35.2	97–104	−0.3–0.3[b]	
Outer Sydney Harbour	2018, May	32.5–35.6	99–101	−0.2–2.2[b]	
Rose Bay	2018, May	32.5–35.3	96–105	−0.4–0.3[b]	
Rozelle Bay	2018, May	30.5–35.5	100–107	0.0–0.8[b]	
Hen and Chicken Bay	2018, May	28.2–32.5	94.5–101.0	−1.5–0.0[b]	
Homebush Bay	2018, May	27.8–32.5	96–168	−0.4–17.7[b]	
Johnstone River estuary	2014, Mar (wet)	<1–12	132–245	0–28.8[b]	
	2014, Sept (dry)	<1–34	97–228	0–17.3[b]	Murray et al. (2020)
Constant Creek estuary	2014, Mar (wet)	11–35	93–104	−1.2–0.7[b]	
	2014, Sept (dry)	30–35	97–132	−0.5–8.2[b]	
Fitzroy River estuary	2014, Mar (wet)	<1–29	100–139	0–14.9[b]	
	2014, Sept (dry)	24–35	103–234	0.2–17.3[b]	
Guadalquivir estuary (Southwestern coast of the Iberian Peninsula)	2017 Jul	0.4–36.5		0.6–130.0[b]	Sánchez-Rodríguez et al. (2022)
	2018 Mar	0.5–33.6		−1.7–59.4[b]	
	2018 Apr	0.8–35.4		−0.9–54.6[b]	
	2019 Mar	0.0–36.3		−2.1–82.9[b]	
	2019 Apr	0.0–35.9		−3.2–113.4[b]	
Danube River plume	1995 July-Aug	0–15	112	2.8[a]	Amouroux et al. (2002)
Mandovi estuary	2011 March-May	11.88–35.18	100.87–270.57	0.04–18.53[b]	Manjrekar et al. (2020)
	2011 June-Sept	0.03–34.58	109.44–2,458.62	1.94–176.75[b]	
	2011 October-Feb	0.07–34.20	99.96–285.88	0.18–7.61[b]	
	2012 March-May	14.39–35.92	109.60–290.44	1.22–39.85[b]	
	2012 June-Sept	0.03–27.67	82.84–1675.8	-	
	2012 October-Feb	6.57–35.01	104.66–238.47	0.45–8.41[b]	
	2013 March-May	24.15–36.33	175.15–258.26	7.93–12.66[b]	

(Continued on following page)

TABLE 3 (*Continued*) N_2O fluxes in rivers and estuaries.

Location	Time	Salinity	N_2O saturation (%)	N_2O flux (μmol m^{-2} d^{-1})	References
	2013 June-Sept	0.05–35.66	149.36–1823.6	3.43–171.12[b]	
	2013 October-Feb	0.08–34.93	139.61–213.11	0.27–4.24[b]	
Cochin estuary	2013 Sept	0.68–3.97	109.00–819.00	2.87–29.73[a]	Hershey et al., 2019)
	2014 Apr	2.13–34.95	53.00–889.00	0.49–26.51[a]	
Yellow River estuary (Before water-sediment regulation)		13–31	94.4–177.7	7.4 ± 4.8[a]	Ma et al. (2016)
Yellow River estuary (During water-sediment regulation)		5–30	123.1–245.7	30.7 ± 19.5[a]	
Yellow River estuary (After water-sediment regulation)		15–29	126.6–245	5.2 ± 2.9[a]	
Changjiang estuary	2002–2006	14–30	137 ± 20	13.3 ± 7.2[a]	Zhang et al. (2010)
Pearl River	2007–2011		450	0.1–733[a]	Lin et al. (2016)
Tamsui River estuary	2019 Nov	0.70–19.07	582–1808	13.3–44.6[a]	This study
				10.9–35.6[b]	
	2020 May	5.69–32.14	244–1101	3.4–18.9[a]	
				2.8–15.1[b]	
	2020 Aug	14.49–33.87	194–679	3.0–12.1[a]	
				2.4–9.5[b]	
	2021 Jan	1.35–33.08	149–1158	2.8–27.3[a]	
				2.8–26.8[b]	

[a]Fluxes were calculated by Wanninkhof (1992) equation.
[b]Fluxes were calculated by Wanninkhof (2014) equation.

mainly influenced by the physical mixing of freshwater and seawater, seasonal changes could not be distinguished here. DO concentrations were influenced by physical mixing, salinity, temperature, and biological status. DO concentration in the estuary was highest in winter (195.2–249.4 μM), followed by autumn (208.4–226.2 μM), summer (141.1–197.0 μM), and spring (106.6–206.3 μM; Table 1). DO saturations exclude the effects of temperature and salinity on gas solubility. It only represents biological conditions and physical mixing. DO saturation in the estuary were similar in autumn (80%–96%), summer (65%–101%), and winter (64%–102%), but lowest in spring (44%–98%; Table 1). In the Tamsui River estuary's adjacent sea, seasonal differences were found in DO concentrations but DO saturations, which reflect the influences of salinity and temperature on DO concentrations.

4.2 Seasonal variations of nutrients and N_2O concentrations in the Tamsui River's adjacent sea

Average surface concentration of NO_2^- was the highest in winter (1.07 ± 0.44 μM), followed by autumn (0.52 ± 0.36 μM), spring (0.36 ± 0.29 μM) and summer (0.33 ± 0.12 μM). Average surface concentration of NO_3^- was the highest in winter (6.7 ± 0.5 μM) followed by autumn (3.8 ± 0.6 μM), spring (1.1 ± 0.9 μM) and summer (1.1 ± 0.6 μM). Seasonal changes in the average surface concentration of PO_4^{3-} showed the same trend as that of NO_3^-. It was the highest in winter (0.61 ± 0.12 μM), followed by autumn (0.37 ± 0.08 μM), spring (0.35 ± 0.20 μM) and summer (0.29 ± 0.11 μM). As the wind was stronger in winter and autumn than in spring and summer (Table 2), vertical mixing would be more intense in winter and autumn than in spring and summer. Vertical mixing resulted in high concentrations of nutrients from the bottom to the surface water; therefore, the average nutrient concentrations in the surface water were higher in winter and autumn than in spring and summer. Surface average N_2O concentrations in four seasons were 13.8 ± 0.9 nM in winter, 11.6 ± 1.2 nM in spring, 11.4 ± 0.7 nM in summer, and 10.3 ± 0.2 in autumn. The dissolved N_2O concentrations in the adjacent sea showed non-significant seasonal variation (Table 1).

4.3 Seasonal variations of nutrients and N_2O concentrations in the Tamsui River estuary

In the estuary, the nutrient distribution was strongly influenced by tides. As salinity represents the tidal effect in the Tamsui River estuary, seasonal changes in nutrients should consider both

TABLE 4 N_2O **fluxes in marine and coastal areas.**

Location	Time	Salinity	N_2O saturation (%)	N_2O flux (μmol m^{-2} d^{-1})	References
North-western Black Sea (open water)	1995 July-Aug	15–18	110	5.2[a]	Amouroux et al. (2002)
North-western Black Sea (shelf water)	1995 July-Aug	>18	112	4.4[a]	
North-eastern shelf of the Gulf of Cádiz (SW Iberian Peninsula)	2006 Jun	36.34 ± 0.08	270 ± 28	25.4 ± 11.3[a]	Ferrón et al. (2010)
	2006 Nov	35.93 ± 0.51	255 ± 34	15.2 ± 11.6[a]	
	2007 Feb	36.02 ± 0.47	125 ± 9	4.7 ± 4.2[a]	
	2007 May	36.04 ± 0.10	120 ± 7	2.2 ± 0.8[a]	
Eastern shelf of the Gulf of Cadiz (SW Iberian Peninsula)	2014 Mar	36.1 ± 0.1	104.1 ± 4.6	2.5 ± 1.4[a]	Sierra et al. (2017)
	2014 Jun	36.2 ± 0.1	117.9 ± 9.0	4.1 ± 3.0[a]	
	2014 Sept	36.1 ± 0.1	125.2 ± 6.1	6.1 ± 3.1[a]	
	2014 Dec	36.3 ± 0.1	98.9 ± 5.3	−1.0 ± 1.2[a]	
	2015 Mar	36.1 ± 0.1	113.4 ± 6.1	2.9 ± 1.2[a]	
	2015 Jun	36.4 ± 0.1	102.5 ± 5.2	1.7 ± 2.0[a]	
	2015 Sept	36.2 ± 0.1	116.4 ± 6.1	2.8 ± 1.2[a]	
	2015 Nov	36.4 ± 0.1	110.6 ± 2.7	2.2 ± 1.7[a]	
Great Barrier Reef (Nearshore)	2014 Jan	35.5 ± 0.06	98.6 ± 0.1	−0.2 ± 0.1[b]	Reading (2022)
Great Barrier Reef (Mid Lagoon)	2014 Jan	35.5 ± 0.01	98.9 ± 0.1	−0.2 ± 0.1[b]	
Great Barrier Reef (Outer Reef)	2014 Jan	35.4 ± 0.02	99.5 ± 0.1	−0.1 ± 0.1[b]	
Bohai Sea	2019 May			2.49 ± 1.49[b]	Gu et al. (2022)
	2019 Aug			9.81 ± 3.52[b]	
	2019 Oct			7.82 ± 2.42[b]	
Jiaozhou Bay (eastern coast)	2002/2003 May			37.3 ± 51.9[a]	Zhang et al. (2006)
	2003 Aug			50.5 ± 27.4[a]	
	2003 Dec			22.4 ± 15.5[a]	
Jiaozhou Bay (western coast)	2003 Aug			43.4 ± 84.8[a]	
	2003 Dec			32.0 ± 41.8[a]	
Jiaozhou Bay (central bay)	2002/2003 May			3.16 ± 7.86[a]	
	2003 Aug			5.81 ± 5.32[a]	
	2003 Dec			−1.31 ± 5.37[a]	
North Yellow Sea	2019 May			2.03 ± 1.74[b]	Gu et al. (2022)
	2019 Aug			7.66 ± 3.24[b]	
	2019 Oct			7.29 ± 3.67[b]	
South Yellow Sea	2019 May			1.19 ± 2.13[b]	
South Yellow Sea	2011 Mar		117 ± 8	4.5 ± 6.5[b]	Chen et al. (2021)
	2011 May		122 ± 5	7.7 ± 4.6[b]	
	2011 Aug		145 ± 13	6.4 ± 5.6[b]	
	2011 Oct		100 ± 8	0.2 ± 0.8[b]	
	2011 Dec		104 ± 11	1.2 ± 2.7[b]	
East China Sea (Shelf area)	2011 Mar		117 ± 14	6.6 ± 9.5[b]	Chen et al. (2021)

(Continued on following page)

TABLE 4 (*Continued*) N_2O fluxes in marine and coastal areas.

Location	Time	Salinity	N_2O saturation (%)	N_2O flux (μmol m^{-2} d^{-1})	References
	2011 May		118 ± 12	6.7 ± 8.0[b]	
	2011 Aug		139 ± 25	8.3 ± 6.7[b]	
	2011 Oct		99 ± 11	−0.2 ± 3.1[b]	
	2011 Dec		110 ± 13	5.1 ± 8.2[b]	
East China Sea (Slope area)	2011 May		114 ± 9	5.6 ± 3.4[b]	
	2011 Oct		86 ± 17	−6.1 ± 7.7[b]	
	2011 Dec		123	13.8[b]	
Changjiang Estuary's adjacent marine area	2002 May	28.9 ± 6.6	141 ± 23	13.2 ± 7.4[a]	Zhang et al. (2010)
	2002 Nov	27.7 ± 5.3	114 ± 25	5.8 ± 10.2[a]	
	2006 Jun	30.6 ± 2.3	119 ± 6	6.1 ± 2.0[a]	
	2006 Aug	31.2 ± 2.2	184 ± 71	32.0 ± 27.1[a]	
	2006 Oct	32.5 ± 1.5	153 ± 24	18.4 ± 8.3[a]	
West Philippines Sea	2004 August 2006 May		90 ± 22	−1.7 ± 3.9[b]	Tseng et al. (2016)
	2007 Jul				
South China Sea	2003 August, Sept		132 ± 23	5.5 ± 3.9[b]	Tseng et al. (2016)
	2004 July 2006 July 2007 Jul				
Tamsui River's adjacent sea area	2019 Nov	33.63 ± 0.10	148 ± 3	45.3 ± 5.1[a], 40.3 ± 0.7[b]	This study
	2020 May	33.71 ± 0.78	183 ± 18	24.1 ± 2.5[a], 19.7 ± 2.1[b]	
	2020 Aug	33.89 ± 0.16	197 ± 12	25.9 ± 1.7[a], 20.9 ± 1.3[b]	
	2021 Jan	33.75 ± 0.53	171 ± 11	60.6 ± 4.1[a], 49.0 ± 3.3[b]	

[a]Fluxes were calculated by Wanninkhof (1992) equation.
[b]Fluxes were calculated by Wanninkhof (2014) equation.

concentration and salinity. The N_2O concentrations followed a descending trend from low to high salinity (Figure 6A). A strong correlation observed in every season indicated that the N_2O concentration in this area was highly influenced by physical mixing. When salinity regressed to zero, N_2O concentration was highest in autumn, followed by winter, spring, and summer (Figure 6A). Hence, without physical mixing, there were seasonal changes in N_2O concentrations in the Tamsui River estuary.

During autumn and winter, DO and NO_3^- concentrations were comparative high among the four seasons. Turner et al. (2016) indicated that NO_3^- is the dominant control on N_2O concentrations but that other environmental variables may limit NO_3^- processing. Many studies have shown that NO_3^- is a parameter that can be used to predict N_2O production (Baulch et al., 2011; Turner et al., 2016), which might be able to explain why N_2O concentrations were higher in autumn and winter when salinity regressed to zero (Figure 6A). Furthermore, the positive correlation between N_2O and NO_3^- during autumn and winter (Figure 7) suggests that the production of N_2O could be attributed to nitrification. (Tseng et al., 2016). A concave downward curve was found in the figure of N_2O concentration *versus* salinity (Figure 6B). This implied that partial riverine N_2O concentrations were removed during transporting to the estuary. In October and November 2019, it was particularly dry compared to other months of sampling in the study, according to the precipitation data from the Central Weather Bureau. As there was a long period of low precipitation before sampling, the water level was low, and the aquatic N_2O concentrations were presumably hugely influenced by the sediment in the Tamsui River estuary. According to Chen et al. (2022), benthic habitats could be a net N_2O sink in the estuary, we assume that the reduction of N_2O concentrations in the water column was influenced by the sediment, however, more research should be done to clarify our hypothesis. The shaded area in Figure 6B shows that the reduction of N_2O concentrations in the water column might be remove by the benthic sediments.

During spring and summer, in the salinity range of 5.69 and 33.87, the concentrations of NO_3^- were extremely low, while NO_2^- and NH_4^+ concentrations were comparably high. Zhang et al. (2020) indicated that NO_3^- and NH_4^+ concentrations were the most important explanatory variables of spatio-temporal variations of N_2O concentration. In spring, NH_4^+ occupied approximately 73% of the DIN proportion with average DO concentration about 160.4 ± 41.9 μM (Figure 8). In summer, NH_4^+ occupied approximately 64% of the DIN proportion with average DO concentration about 178.2 ± 22.8 μM (Figure 8). N_2O reduction has traditionally been considered active only under extremely low oxygen concentrations or in anoxic environments (Miller et al., 1986; Naqvi et al., 2000; Dalsgaard et al., 2014; Babbin et al., 2015). However, recent studies have found that N_2O reduction may occur in oxygenated waters (Wyman et al., 2013; Raes et al., 2016; Sun et al., 2017; Rees et al., 2021; Sun et al., 2021; Tang et al., 2022). Based on the findings of Tang et al. (2022), it appears that reducing the DO concentration can trigger N_2O reduction, and the rates of N_2O reduction were observed to vary with the DO concentration levels. Despite the fact that the highest N_2O reduction rates were observed when DO was depleted (DO concentrations were close to 0 μM), N_2O reduction still occurred even when DO concentration was as high as 215 μM (Tang et al., 2022). Tang et al. (2022) also made the point that the steep gradient of oxygen and its dynamic changes in estuaries can expose microbes to varying oxygen conditions, promoting the survival and growth of N_2O-reducing microbes that are adapted to different oxygen levels or tolerant of a range of oxygen levels. This implies that even though DO is never fully depleted, denitrification can still take place. According to Xiang et al. (2022), a warm environment is more conducive to denitrification. This could explain why, out of all seasons, N_2O concentrations tend to be lower in summer and spring due to the warm temperatures that favor this loss pathway.

4.4 N_2O fluxes in the Tamsui River estuary and its adjacent sea

Two important factors that might affect sea-to-air N_2O fluxes are wind speed and dissolved N_2O concentrations. In this study, monthly average wind speeds in Tamsui and Taipei Harbor were used to calculate sea-to-air N_2O fluxes in the Tamsui River estuary and its adjacent sea, respectively. In both the Tamsui River estuary and its adjacent sea, wind speeds were higher in autumn and winter than in spring and summer (Table 2). Although sea-to-air N_2O fluxes showed similar seasonal variation in both the Tamsui River estuary and its adjacent sea, the main factors that influenced sea-to-air N_2O fluxes were different. We observe a greater seasonal variation of wind speed in adjacent sea (5.0–8.0 m/s) than in the estuary (1.6–2.0 m/s). Because of the occlusion of mountains, the seasonal wind speed varied less in the Tamsui River estuary than in the adjacent sea. In contrast, dissolved N_2O concentrations showed greater seasonal variations in the Tamsui River estuary than in the adjacent sea. This implies that seasonal variations in N_2O fluxes in the estuary were dominated by N_2O concentrations in the water, whereas in the sea, it was dominated by wind speed. Overall, the Tamsui River estuary and its adjacent sea were net sources of atmospheric N_2O with annual average fluxes 10.6 ± 6.7 and 32.5 ± 14.5 μmol m^{-2} d^{-1}, respectively.

The area of the Tamsui River estuary (Figure 1) is about 10.3 km^2. Assuming the highest seasonal N_2O flux, the Tamsui River estuary would have emitted approximately 0.08 × 10^6 mol of N_2O into the atmosphere annually. The Tamsui River is shallow with an average annual flow rate of 6,968 × 10^6 m^3 (Wang et al., 2014). According to the Hydrological Year Book of Taiwan (2021), 64% of water flow occurred between May and October (data between 1949–2021). The concentration of N_2O in the estuary varied seasonally and was impacted by physical mixing with seawater. To estimate the N_2O concentrations at a salinity of 0 for each season, we utilized a graph that depicts the concentration of N_2O as a function of salinity. By factoring in the seasonal riverine N_2O concentrations and river flow rates, we computed an annual advective transport of N_2O of approximately 0.71 × 10^6 mol. As a result, the annual advective transport of N_2O to the sea was about 9 times more than the vertical transport of N_2O to the atmosphere in the Tamsui River estuary. This implies that by reducing N_2O loading in the river, we can not only minimize N_2O emissions within the river and estuary, but also decrease the amount of residual riverine N_2O that is transported to the sea, where it can escape into the atmosphere.

4.5 N_2O concentrations and water-to-air fluxes in world estuaries and their adjacent sea

N_2O showed higher concentrations upstream of the river or at tributary interchange site. In addition, urban rivers showed higher N_2O fluxes than rural rivers, providing evidence that anthropogenic activities have increased emissions of N_2O (Murray et al., 2020; Reading et al., 2020; Reading, 2022). According to previous research (Murray et al., 2020; Reading et al., 2020; Reading, 2022), N_2O saturations varied over a range of 77.7%–677.7% and N_2O fluxes varied over a range of −2.8–120.9 μmol m^{-2} d^{-1} in Australia's rivers and estuaries. For rivers and estuaries near European country, N_2O fluxes ranged between −3.2–130.0 μmol m^{-2} d^{-1} (Amouroux et al., 2002; Sánchez-Rodríguez et al., 2022). In India, studies on N_2O fluxes are often discussed with regards to the effect of the southwest monsoon. In the Mandovi estuary, N_2O fluxes were highest during the southwest monsoon (June to September) with a range of 1.94–176.75 μmol m^{-2} d^{-1}. This shows that wind speed is a strong factor affecting fluxes of N_2O (Manjrekar et al., 2020). N_2O fluxes from rivers and estuaries in Asia ranged between 0.1 and 733 μmol m^{-2} d^{-1}. The N_2O fluxes from the Pearl River were the highest (Lin et al., 2016) among the studies considered in this research. Compared with other rivers and estuaries, N_2O fluxes in the Tamsui River estuary were slightly higher than those of most estuaries (Table 3), especially those rivers and estuaries in Australia that remain undeveloped. N_2O fluxes in the Tamsui River estuary (2.8–44.6 μmol m^{-2} d^{-1}) were higher than those of most rural rivers, but lower than those of some urban rivers or rivers that are affected by the monsoon. Observed N_2O saturations in Tamsui River estuary (149%–1808%) were higher than the mean value 602% for the global estuaries (Bange et al., 1996). Anthropogenic activities in the Tamsui River estuary increased N_2O concentrations in the water and emissions from water to the atmosphere. As Tamsui River estuary is surrounding by mountains and high buildings, it blocks the wind to the estuary. Although the N_2O concentrations were high in the Tamsui River estuary, the advective transport of N_2O to the sea was much higher than the vertical transport of N_2O to the atmosphere.

Table 4 shows N_2O fluxes from marine and coastal area. The lowest average N_2O fluxes was −1.0 ± 1.2 μmol m^{-2} d^{-1} at eastern shelf of the Gulf of Cadiz and the highest average N_2O fluxes was 25.4 ± 11.3 μmol m^{-2} d^{-1} at north-eastern shelf of the Gulf of Cadiz (Ferrón et al., 2010; Sierra et al., 2017). At Eastern shelf of the Gulf of Cadiz, the highest concentration of N_2O was found at the shallower stations, indicating coastal input and benthic remineralization that are sources of N_2O in coastal area (Sierra et al., 2017). Studies in Great Barrier Reef showed that it is a sink for atmospheric N_2O with the flux of −0.2 ± 0.1 μmol m^{-2} d^{-1} (Reading, 2022). The West Philippines Sea is also a sink of N_2O with an average N_2O flux −1.7 ± 3.9 μmol m^{-2} d^{-1}

(Tseng et al., 2016). N_2O fluxes from Chinese coastal waters were sources to atmosphere. N_2O high fluxes were observed in Jiaozhou Bay which usually average at 50.5 ± 27.4 μmol m^{-2} d^{-1} at its eastern coast (Zhang et al., 2006). N_2O concentrations and fluxes of the Tamsui River estuary's adjacent sea were higher than most of the marine and coastal areas. Anthropogenic activities in the urban estuary, coupled with the terrain geography of the basin, may be the underlying cause of this issue. The blocked wind movement in the basin has resulted in the majority of N_2O being transferred to the sea, rather than the atmosphere. Overall, N_2O saturations from our study (148% ± 3% to 197% ± 12%) were higher than the mean value 109% for the global coastal waters (Bange et al., 1996).

5 Conclusion

A descending trend in N_2O concentrations was observed in four seasons from the Tamsui River estuary to its adjacent sea, mainly due to physical mixing. During autumn and winter, higher DO and NO_3^- concentrations might result in higher N_2O concentrations. In addition, there was a concave downward curve in the relationship between N_2O concentration and salinity, which implied that partial N_2O concentrations in the water column were removed during transportation. In spring and summer, lower DO and higher water temperatures might be more suitable for denitrification microbes, which results in lower N_2O concentrations compared to those in autumn and winter. N_2O concentrations showed greater seasonal variations in the Tamsui River estuary than in the adjacent sea. However, wind speeds varied less seasonally in the Tamsui River estuary than in the adjacent sea. As a result, seasonal variations in N_2O fluxes in the estuary were dominated by N_2O concentrations in the water, whereas in the sea, it was dominated by wind speed. Overall, the Tamsui River estuary and its adjacent sea were net sources of atmospheric N_2O with annual average fluxes 10.6 ± 6.7 and 32.5 ± 14.5 μmol m^{-2} d^{-1}, respectively.

Data availability statement

The datasets presented in this study can be found in online repositories. The names of the repository/repositories and accession number(s) can be found in the article/Supplementary material.

Author contributions

H-CT developed the idea of the study. H-CT leaded the research cruises and did the sampling. C-CL, YTYH and G-CG analyzed the samples and data. H-CT and YTYH wrote the first draft of the article and all authors contributed equally to the interpretation of the results and in writing the final manuscript.

Funding

This research was supported by the Ministry of Science and Technology of the ROC, Taiwan (MOST 108-2611-M-019-021-MY3).

Acknowledgments

The authors wish to thank the Ministry of Science and Technology of the ROC, Taiwan for supporting this research, and the captain and crews of Ocean Researcher 2 and New Ocean Researcher 2 for their assistance. We thank three reviewers for their constructive and detailed comments to strengthen the manuscript.

Conflict of interest

The authors declare that the research was conducted in the absence of any commercial or financial relationships that could be construed as a potential conflict of interest.

Publisher's note

All claims expressed in this article are solely those of the authors and do not necessarily represent those of their affiliated organizations, or those of the publisher, the editors and the reviewers. Any product that may be evaluated in this article, or claim that may be made by its manufacturer, is not guaranteed or endorsed by the publisher.

References

Amouroux, D., Roberts, G., Rapsomanikis, S., and Andreae, M. O. (2002). Biogenic gas (CH4, N2O, DMS) emission to the atmosphere from near-shore and shelf waters of the north-Western black sea. *Estuar. Coast. Shelf Sci.* 54, 575–587. doi:10.1006/ecss.2000.0666

Babbin, A. R., Bianchi, D., Jayakumar, A., and Ward, B. B. (2015). Rapid nitrous oxide cycling in the suboxic ocean. *Science* 348, 1127–1129. doi:10.1126/science.aaa8380

Bange, H. W., Rapsomanikis, S., and Andreae, M. O. (1996). Nitrous oxide in coastal waters. *Glob. Biogeochem. Cycles* 10, 197–207. doi:10.1029/95gb03834

Baulch, H. M., Schiff, S. L., Maranger, R., and Dillon, P. J. (2011). Nitrogen enrichment and the emission of nitrous oxide from streams. *Glob. Biogeochem. Cycles* 25, n/a. doi:10.1029/2011gb004047

Chen, J. J., Wells, N. S., Erler, D. V., and Eyre, B. D. (2022). Land-use intensity increases benthic N2O emissions across three sub-tropical estuaries. *J. Geophys. Res. Biogeosciences* 127. doi:10.1029/2022jg006899

Chen, X., Ma, X., Gu, X., Liu, S., Song, G., Jin, H., et al. (2021). Seasonal and spatial variations of N2O distribution and emission in the east China sea and south yellow sea. *Sci. Total Environ.* 775, 145715. doi:10.1016/j.scitotenv.2021.145715

Dalsgaard, T., Stewart, F. J., Thamdrup, B., De Brabandere, L., Revsbech, N. P., Ulloa, O., et al. (2014). Oxygen at nanomolar levels reversibly suppresses process rates and gene expression in anammox and denitrification in the oxygen minimum zone off northern Chile. *mBio* 5, e01966. doi:10.1128/mbio.01966-14

Ferrón, S., Ortega, T., and Forja, J. M. (2010). Nitrous oxide distribution in the north-eastern shelf of the Gulf of Cádiz (SW Iberian Peninsula). *Mar. Chem.* 119, 22–32. doi:10.1016/j.marchem.2009.12.003

Gu, T., Jia, D., Wang, Z., Guo, Y., Xin, Y., Guo, C., et al. (2022). Regional distribution and environmental regulation mechanism of nitrous oxide in the Bohai sea and north yellow sea: A preliminary study. *Sci. Total Environ.* 818, 151718. doi:10.1016/j.scitotenv.2021.151718

Hydrological Year Book of Taiwan (2021). *Water resources agency, ministry of economic affairs, June 2022*, 1078. Taipei, Taiwan.

IPCC (2013). Carbon and other biogeochemical cycles. In *Contribution of Working Group I to the Fifth Assessment Report of the Intergovernmental Panel on Climate Change*. Editors T. F. Stocker, D. Qin, G.-K. Plattner, M. Tignor, S. K. Allen, J. Boschung, et al. (Cambridge, United Kingdom and New York, NY, USA: Cambridge University Press).

IPCC (2021). Changing state of the climate system. In *Climate change 2021: The physical science basis. Contribution of working group I to the sixth assessment Report of the intergovernmental Panel on climate change*, V. masson-delmotte, P. Zhai, A. Pirani, S. L. Connors, C. Péan, S. Berger, N. Caud, et al. (Cambridge, United Kingdom and New York, NY, USA: Cambridge University Press). 287–422.

Lin, H., Dai, M., Kao, S.-J., Wang, L., Roberts, E., Yang, J.-Y. T., et al. (2016). Spatiotemporal variability of nitrous oxide in a large eutrophic estuarine system: The Pearl River Estuary, China. *Mar. Chem.* 182, 14–24. doi:10.1016/j.marchem.2016.03.005

Ma, X., Zhang, G.-L., Liu, S.-M., Wang, L., Li, P.-P., Gu, P.-P., et al. (2016). Distributions and fluxes of nitrous oxide in lower reaches of Yellow River and its estuary: Impact of water-sediment regulation. *Estuar. Coast. Shelf Sci.* 168, 22–28. doi:10.1016/j.ecss.2015.10.001

Manjrekar, S., Uskaikar, H., and Morajkar, S. (2020). Seasonal production of nitrous oxide in a tropical estuary, off Western India. *Regional Stud. Mar. Sci.* 39, 101418. doi:10.1016/j.rsma.2020.101418

Miller, L. G., Oremland, R. S., and Paulsen, S. (1986). Measurement of nitrous oxide reductase activity in aquatic sediments. *Appl. Environ. Microbiol.* 51, 18–24. doi:10.1128/aem.51.1.18-24.1986

Murphy, J., and Riley, J. P. (1962). A modified single solution method for the determination of phosphate in natural waters. *Anal. Chim. Acta* 27, 31–36. doi:10.1016/s0003-2670(00)88444-5

Murray, R., Erler, D., Rosentreter, J., Wells, N., and Eyre, B. (2020). Seasonal and spatial controls on N2O concentrations and emissions in low-nitrogen estuaries: Evidence from three tropical systems. *Mar. Chem.* 221, 103779. doi:10.1016/j.marchem.2020.103779

Naqvi, S. W. A., Jayakumar, D. A., Narvekar, P. V., Naik, H., Sarma, V. V. S. S., D'Souza, W., et al. (2000). Increased marine production of N2O due to intensifying anoxia on the Indian continental shelf. *Nature* 408, 346–349. doi:10.1038/35042551

Pai, S.-C., Gong, G.-C., and Liu, K.-K. (1993). Determination of dissolved oxygen in seawater by direct spectrophotometry of total iodine. *Mar. Chem.* 41, 343–351. doi:10.1016/0304-4203(93)90266-q

Pai, S.-C., Tsau, Y.-J., and Yang, T.-I. (2001). pH and buffering capacity problems involved in the determination of ammonia in saline water using the indophenol blue spectrophotometric method. *Anal. Chim. Acta* 434, 209–216. doi:10.1016/s0003-2670(01)00851-0

Pai, S.-C., Yang, C.-C., and Riley, J. P. (1990a). Effects of acidity and molybdate concentration on the kinetics of the formation of the phosphoantimonylmolybdenum blue complex. *Anal. Chim. Acta* 229, 115–120. doi:10.1016/s0003-2670(00)85116-8

Pai, S.-C., Yang, C.-C., and Riley, J. P. (1990b). Formation kinetics of the pink azo dye in the determination of nitrite in natural waters. *Anal. Chim. Acta* 232, 345–349. doi:10.1016/s0003-2670(00)81252-0

Raes, E. J., Bodrossy, L., Van de Kamp, J., Holmes, B., Hardman-Mountford, N., Thompson, P. A., et al. (2016). Reduction of the powerful greenhouse gas N2O in the south-eastern Indian ocean. *PLoS One* 11, e0145996. doi:10.1371/journal.pone.0145996

Ravishankara, A. R., Daniel, J. S., and Portmann, R. W. (2009). Nitrous oxide (N2O): The dominant ozone-depleting substance emitted in the 21st century. *Science* 326, 123–125. doi:10.1126/science.1176985

Reading, M. J. (2022). *Aquatic nitrous oxide dynamics from rivers to reefs*. Southern Cross University.

Reading, M. J., Tait, D. R., Maher, D. T., Jeffrey, L. C., Looman, A., Holloway, C., et al. (2020). Land use drives nitrous oxide dynamics in estuaries on regional and global scales. *Limnol. Oceanogr.* 65, 1903–1920. doi:10.1002/lno.11426

Rees, A. P., Brown, I. J., Jayakumar, A., Lessin, G., Somerfield, P. J., and Ward, B. B. (2021). Biological nitrous oxide consumption in oxygenated waters of the high latitude Atlantic Ocean. *Commun. Earth Environ.* 2, 36. doi:10.1038/s43247-021-00104-y

Sánchez-Rodríguez, J., Sierra, A., Jiménez-López, D., Ortega, T., Gómez-Parra, A., and Forja, J. (2022). Dynamic of CO2, CH4 and N2O in the Guadalquivir estuary. *Sci. Total Environ.* 805, 150193. doi:10.1016/j.scitotenv.2021.150193

Seitzinger, S. P., and Kroeze, C. (1998). Global distribution of nitrous oxide production and N inputs in freshwater and coastal marine ecosystems. *Glob. Biogeochem. Cycles* 12, 93–113. doi:10.1029/97gb03657

Sierra, A., Jiménez-López, D., Ortega, T., Ponce, R., Bellanco, M. J., Sánchez-Leal, R., et al. (2017). Distribution of N2O in the eastern shelf of the Gulf of Cadiz (SW iberian peninsula). *Sci. Total Environ.* 593-594, 796–808. doi:10.1016/j.scitotenv.2017.03.189

Strickland, J. D. H., and Parsons, T. R. (1972). *A practical handbook of seawater analysis*. Ottawa, Canada: Fisheries Research Board of Canada, 310.

Sun, X., Jayakumar, A., Tracey, J. C., Wallace, E., Kelly, C. L., Casciotti, K. L., et al. (2021). Microbial N2O consumption in and above marine N2O production hotspots. *ISME J.* 15, 1434–1444. doi:10.1038/s41396-020-00861-2

Sun, X., Jayakumar, A., and Ward, B. B. (2017). Community composition of nitrous oxide consuming bacteria in the oxygen minimum zone of the eastern tropical south pacific. *Front. Microbiol.* 8, 1183. doi:10.3389/fmicb.2017.01183

Tang, W., Jayakumar, A., Sun, X., Tracey, J. C., Carroll, J., Wallace, E., et al. (2022). Nitrous oxide consumption in oxygenated and anoxic estuarine waters. *Geophys. Res. Lett.* 49. doi:10.1029/2022gl100657

Tian, H., Xu, R., Canadell, J. G., Thompson, R. L., Winiwarter, W., Suntharalingam, P., et al. (2020). A comprehensive quantification of global nitrous oxide sources and sinks. *Nature* 586, 248–256. doi:10.1038/s41586-020-2780-0

Tseng, H.-C., Chen, C.-T. A., Borges, A. V., DelValls, T. A., Lai, C.-M., and Chen, T.-Y. (2016). Distributions and seasea-to-air fluxes of nitrous oxide in the south China sea and the west Philippines sea. *Deep Sea Res. Part I Oceanogr. Res. Pap.* 115, 131–144. doi:10.1016/j.dsr.2016.06.006

Tseng, H.-C., Newton, A., Gong, G.-C., and Lin, C.-C. (2021). Social–environmental analysis of estuary water quality in a populous urban area. *Elem. Sci. Anthropocene* 9, 1. doi:10.1525/elementa.2020.00085

Turner, P. A., Griffis, T. J., Baker, J. M., Lee, X., Crawford, J. T., Loken, L. C., et al. (2016). Regional-scale controls on dissolved nitrous oxide in the Upper Mississippi River. *Geophys. Res. Lett.* 43, 4400–4407. doi:10.1002/2016gl068710

Wanninkhof, R. (2014). Relationship between wind speed and gas exchange over the ocean revisited. *Limnol. Oceanogr. Methods* 12, 351–362. doi:10.4319/lom.2014.12.351

Weiss, R. F. (1981). Determinations of carbon dioxide and methane by dual catalyst flame lonization chromatography and nitrous oxide by electron capture chromatography. *J. Chromatogr. Sci.* 91, 612–616. doi:10.1093/chromsci/19.12.611

Weiss, R. F., and Price, B. A. (1980). Nitrous oxide solubility in water and seawater. *Mar. Chem.* 8, 347–359. doi:10.1016/0304-4203(80)90024-9

Wen, L.-S., Jiann, K.-T., and Liu, K.-K. (2008). Seasonal variation and flux of dissolved nutrients in the danshuei estuary, taiwan: A hypoxic subtropical mountain river. *Coast. Shelf Sci.* 78, 694–704. doi:10.1016/j.ecss.2008.02.011

Wyman, M., Hodgson, S., and Bird, C. (2013). Denitrifying alphaproteobacteria from the Arabian Sea that express nosZ, the gene encoding nitrous oxide reductase, in oxic and suboxic waters. *Appl. Environ. Microbiol.* 79, 2670–2681. doi:10.1128/aem.03705-12

Xiang, H., Hong, Y., Wu, J., and Long, A. (2022). Ecological distribution and diversity of key functional genes for denitrification in surface sediments of the northern south China sea: Implications for potential N2O emissions. *Front. Mar. Sci.* 9. doi:10.3389/fmars.2022.912402

Zhang, G. L., Zhang, J., Liu, S. M., Ren, J. L., and Zhao, Y. C. (2010). Nitrous oxide in the Changjiang (Yangtze River) Estuary and its adjacent marine area: Riverine input, sediment release and atmospheric fluxes. *Biogeosciences* 7, 3505–3516. doi:10.5194/bg-7-3505-2010

Zhang, G., Zhang, J., Xu, J., and Zhang, F. (2006). Distributions, sources and atmospheric fluxes of nitrous oxide in Jiaozhou Bay. *Estuar. Coast. Shelf Sci.* 68, 557–566. doi:10.1016/j.ecss.2006.03.007

Zhang, W., Li, H., Xiao, Q., Jiang, S., and Li, X. (2020). Surface nitrous oxide (N2O) concentrations and fluxes from different rivers draining contrasting landscapes: Spatio-temporal variability, controls, and implications based on IPCC emission factor. *Environ. Pollut.* 263, 114457. doi:10.1016/j.envpol.2020.114457